

Kirigami layer jamming

Robert Baines, Bilige Yang, Luis A. Ramirez, Rebecca Kramer-Bottiglio *

Yale University, United States of America

ARTICLE INFO

Keywords:

Soft robotics
Laminar jamming
Variable stiffness

ABSTRACT

Variable stiffness materials bridge the desirable qualities of soft and rigid robotic components, forming the basis of new machines that contextually adapt their structural properties. Recent developments have led to the creation of jamming materials: Collections of media that undergo pressure-dependent kinematic and frictional interactions to radically, rapidly, and reversibly change in stiffness. Among the types of jamming, laminar jamming harnesses an ensemble of sheets for stiffness changes. Most implementations of laminar jamming employ unaltered, continuous sheets, though the vast design space of mechanical anisotropy programmed via structured cuts invites a new jamming paradigm: kirigami laminar jamming. Through analytical, experimental, and numerical studies, we show how intentional topological augmentation of laminar jamming sheets through shell, void, and cut geometric primitives can elicit bespoke mechanical responses. In particular, we optimize jamming specimens to enhance the jammed to unjammed flexural stiffness ratio across a range of deflections, which unlocks new move-and-hold capabilities. We also demonstrate pressure-induced shape morphing and both sharp-edged and doubly-curved surface matching with kirigami patterns. Results hold broad significance for robotics, morphing structures, and the systematic design of variable stiffness materials.

The boundaries between traditional material paradigms in robotics – soft and rigid – are beginning to dissolve: Variable stiffness materials grant machines seemingly incongruous compliance and load-bearing properties that may be switched on demand to adapt them to multifarious environments and tasks [1–5]. A wide array of variable stiffness materials employed in robotics harnesses changes in intrinsic material properties, geometry, and sometimes both in tandem, to elicit programmed stiffness differentials. Examples include shape memory alloys [6,7], low melting-point alloys [8,9], electrostatic clutches [10, 11], and jamming systems [12,13].

The past few years have witnessed jamming systems emerge as a particularly effective solution for variable stiffness robot components, due to their high stiffness differentials over rapid timescales, ease of manufacture, lack of toxic and leaky components, and amenability to various form factors [13–17]. Jamming systems typically employ a vacuum to trigger increases in kinematic and frictional interactions within a closed domain of material, resulting in stiffness changes [18]. There are several classes of jamming systems, including granular, fiber, tensile fiber, laminar, and stretchable laminar. Each class is distinguished by a distinct form factor and the configuration of its constituent materials. Different deformation mechanics, theoretical stiffness differential ranges, and favorable loading conditions have therefore been observed among the classes of jamming [12].

Laminar (layer) jamming harnesses stiffness changes that result from the compression of a collection of sheets into a cohesive beam-like

cross section [19,20]. Among all classes of jamming, laminar jamming offers the benefits of a thin profile, highly reversible stiffness transitions, and favorable scaling of the stiffness differential by increasing the number of layers [21]. However, the unjammed flexural stiffness increases as the cube of the sheets' thicknesses and proportionally to the number of sheets. The restoring bending moment and shear force through the stack of sheets therefore become higher for a given deflection. For assemblies composed of many thick sheets, move-and-hold ability, describing shape retention of the jammed structure (i) after its initial forming load is released, and (ii) upon application of external loads, may consequently be compromised, because the assembly of sheets will tend to spring back flat rather than retain a deflected configuration. As a concrete example, consider bending a rectangular jamming specimen about its short axis 180° into a smooth arc. With design parameters of fifteen neat (unaltered) Polyethylene Terephthalate (PET) sheets, each dimensioned 0.25 mm thick, 50 mm wide, and 150 mm long, the specimen is unable to hold the desired shape when jammed (Video S1). Another limitation of traditional laminar jamming is that move-and-hold operations are limited to smooth, single-curvature bending deformations.

Several methods have been proposed to tune the mechanics of laminar jamming structures and expand their versatility. For instance, jamming sandwich structures use lightweight, compliant material as

* Corresponding author.

E-mail address: rebecca.kramer@yale.edu (R. Kramer-Bottiglio).

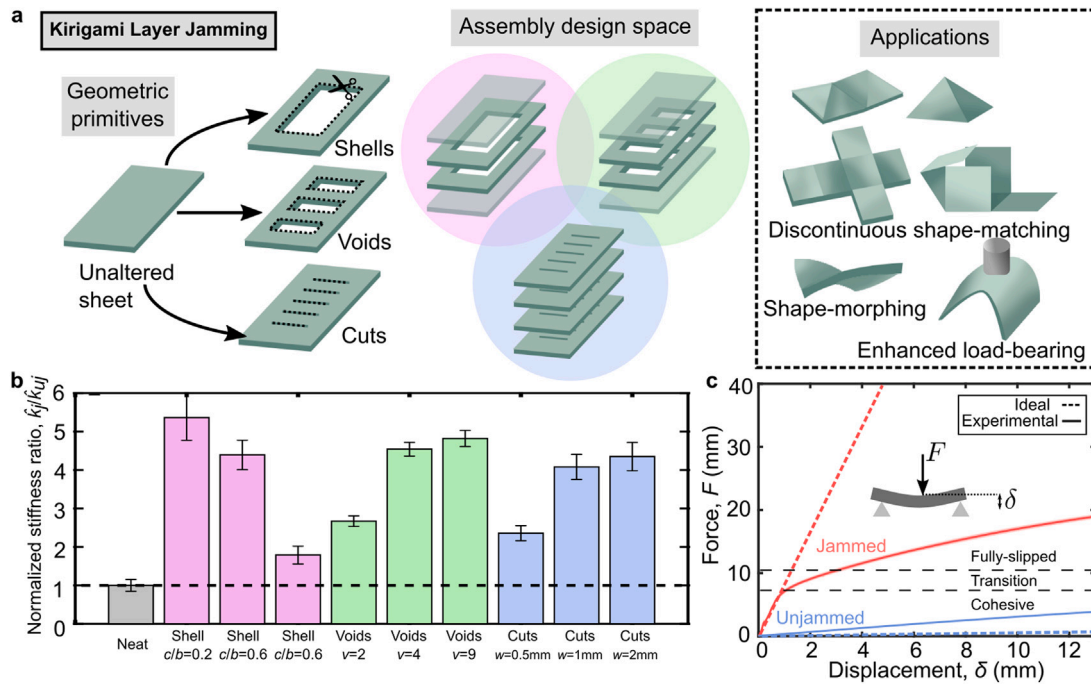


Fig. 1. Kirigami layer jamming. a. Augmenting sheets of laminar jamming systems with various types of structured cuts enables new and improved variable stiffness material functionality, including discontinuous shape-matching, self-morphing, and enhanced load-bearing. b. Summary of initial flexural stiffness ratio amplification due to kirigami layer jamming. X-axis categorical labels represent layer jamming specimens with design parameters that are evaluated in this manuscript. Parameters c/b , v , and w are defined in Fig. 2a, Fig. 3a, and Fig. 4a, respectively. The jammed to unjammed initial stiffness ratio is normalized by that of the neat specimen. Chart plots a mean of five samples; error bars indicate one standard deviation from the mean. c. A canonical three-point bending plot of a neat laminar jamming specimen, characterized by three regimes: cohesive, in which the sheets collectively act as a solid beam, transition, in which the sheets begin to slip relative to one another, and fully-slipped, during which constant sliding of sheets and substantial energy dissipation occurs. The dashed line juxtaposes a hand-drawn hypothetical performance of an ideal laminar jamming system that maintains high stiffness at large deflections, and exhibits substantially less unjammed stiffness than jammed stiffness. We step toward the ideal system by evoking kirigami techniques.

the interior layers and stiffer material as the outer layers to amplify stiffness ratios [22]. The same work also suggests increasing porosity of the center materials to further increase stiffness ratios. Jamming structures using honeycomb [23,24] or cellular [25] composites employ a single block of material with patterned cuts sandwiched by a number of elastic sheets. These architectures allow for distributed curvatures and enhanced jamming ratios, yet occupy a large volume compared to discrete sheet assemblies. Other work demonstrates how identical cuts through all layers can create jammed forms with anisotropic stiffness properties [12,26]. Woven and folded laminar jamming structures are likewise amenable to creation of jammed faceted shapes [26], and stretchable laminar jamming – cutting a single sheet into multiple discretely anchored, interleaved sheets – presents a way to accommodate doubly-curved surfaces [27]. Despite recent progress, no work to-date has systematically analyzed the design space of cut contiguous sheets that are easy to manufacture, require only one type of material, and amplify flexural stiffness changes compared to discretely anchored or neat sheet constituents.

Harnessing the mechanical anisotropy of kirigami [28,29], we introduce *kirigami layer jamming*: strategic removal of material through structured cuts to modify contiguous sheets' second moment of area, contact mechanics, and stretchability, and induce internal curvatures when the constituents are under vacuum (Fig. 1a). Although historically a technique for creating forms from folded and cut paper, research communities have adopted the term “kirigami” to describe use of cuts in tuning the stiffness of materials [30]. We study kirigami layer jamming via minimal analytical models, experiments, and finite element analysis (FEA) to quantify the influence of key design parameters on the mechanical response under loading in a three-point bending setup. We find that kirigami primitives including shells, voids, and cuts allow programming of specimens' jammed and unjammed flexural stiffnesses over wide deflection ranges, enabling new mechanical functionality and significant amplification of stiffness ratios relative to neat specimens

(Fig. 1b). Demonstrations employing kirigami layer jamming attest to its robotic and structural utility compared to neat layer jamming for discontinuous shape matching and move-and-hold load-bearing operations. Moreover, we demonstrate how topological augmentations can give rise to pressure-induced shape-morphing, or stretching to approximate Gaussian-curved topography, expanding the repertoire of functionality in layer jamming systems. This work not only presents a rapid, predictable, and scalable solution for variable stiffness robotic components, but provides a rigorous theoretical and empirical foundation for how geometry influences performance in variable stiffness material design.

1. Results and discussion

1.1. Motivation

To contextualize the effects of kirigami augmentations to laminar jamming systems, we start by considering the force–displacement behavior of neat jammed layers during a three-point bending test. The behavior can be split into three regimes: pre-slip, transition, and fully-slipped (Fig. 1c) [19]. In the pre-slip regime, the layers remain cohesive. Consequently, the jammed flexural stiffness, k_j , is relatively high. During the transition regime, the longitudinal shear stress begins to exceed the maximum possible shear stress determined by the pressure and friction between the layers. A decrease in stiffness thus occurs in the force–displacement relations at larger deflections. The fully-slipped regime is characterized by constant movement of layers relative to one another and a flexural stiffness akin to that of the unjammed state, k_u .

For variable stiffness materials, it is desired to modulate between extremes of rigidity and compliance, in order to reap the benefits of both load-bearing and shape-shifting in robotics applications. An ideal laminar jamming system would therefore not only accommodate

diverse shape-morphing operations, but maximize the ratio of jammed to unjammed flexural stiffnesses, *i.e.* $\max(k_j/k_{uj})$, over a wide deflection range. We can divide this ideal behavior into two testable design objectives: (i) elicit high initial k_j/k_{uj} , and (ii) prevent a drop in jammed stiffness during the transition regime. Scaling analysis provides quantitative framing for these objectives. Treating the jamming system in three-point bending as an Euler–Bernoulli beam with a rectangular cross section described by a width of b , individual layer height of h , and number of layers N , the pre-slip regime stiffness ratio is given by (Note S1):

$$k_j/k_{uj} \approx I_j/I_{uj} = N^2 \quad (1)$$

Here, $I_j = \frac{1}{12}bh^3N^3$ and $I_{uj} = \frac{1}{12}bh^3N$ are the jammed and unjammed cross sections' second moments of area, respectively. The transverse load at slip, V_{max} , scales proportionally to the static coefficient of friction μ , pressure P , and area of the cross section $A = bNh$.

1.2. Shelling

According to the above scaling arguments for neat layers, it is immediately clear that k_j/k_{uj} increases with N [19,31]. Another approach to increase k_j/k_{uj} – requiring no additional material – would be to directly tune the second moments of area of the cross sections in their jammed and unjammed states, such that additional terms remain besides N^2 when computing the ratio. Consider “shelling” the jamming structure by removing an amount of material of width c from the middle of a layer's total width b . We impose the shelling operation to effect q layers and to be symmetric about the neutral axis of the cohesive system, enforcing N, q as both odd or even integers. We effectively augment the sheets' aggregate cross section to become a hollow rectangle (Fig. 2a). The jammed stiffness becomes:

$$I_j = \frac{1}{12}bh^3N^3 - \frac{1}{12}ch^3q^3 \quad (2)$$

The unjammed stiffness becomes:

$$I_{uj} = \frac{1}{12}bh^3N - \frac{1}{12}ch^3q \quad (3)$$

Their ratio is thus:

$$I_j/I_{uj} = R = \frac{bN^3 - cq^3}{bN - cq} \quad (4)$$

Eqs. (1) and (4) indicate that $R > N^2$ for all shelled specimens with valid design parameters. In other words, shelling always increases k_j/k_{uj} relative to a neat specimen of the same boundary geometry. Extremizing R with respect to q yields shelled jamming design parameters that satisfy $\max(k_j/k_{uj})$ (Note S2; Fig. S1a). Based on this extremization, we expect that specimens with c toward the limit of b and q toward the limit of N will elevate k_j/k_{uj} .

The theoretical impact of shelling operations on the transition regime can be understood by setting the maximum sustainable shear stress equal to the longitudinal shear induced by loading, and solving for the resultant force, V_s , that would initiate slip. The equation for V_s suggests increasing c to the limit of b and q to the limit of N will cause slip to occur earlier (Note S2; Fig. S1b). Theoretical modeling thus indicates that design choices for $\max(k_j/k_{uj})$ may counteract design choices for higher V_s , and vice-versa.

In actuality, when a shelled specimen is jammed, it does not retain a perfect hollow rectangular cross section. Jamming pressure causes the unaltered top and bottom sheets to bow into the empty volume created by shelling. To study the influence of design parameters on the resulting cross section, we fabricated several laminar jamming specimens for combinations of $c/b = 0.2, 0.6$, and 0.8 , and $q = 3, 5$, and the optimal number shelled layers based on the other dimensions and given by the maximum of Eq. (4). We consider here the cases of varying c/b with fixed q at the optimal values (See Note S2 and Fig. S2 for discussion of subsequent experiments varying q). Surface profilometry indicates

the emergence of topographical depressions in the shelled specimens that increase in area with increasing c/b (Fig. 2b–d). Profilometry slices verify there is curvature induced by the top and bottom layers bowing into the empty volume (Fig. 2e–g black lines). The curvature is not constant and eventually vanishes at a flat contact interface formed by the meeting of the top and bottom layers.

We developed a model that yielded qualitatively similar interface shapes to actual specimens (Note S2; Fig. 2e–g blue lines). The model projects that the second moments of area will decrease by 0.1%, 47%, and 70% relative to an un-deformed cross section for optimal specimens with $c/b = 0.2, 0.6$, and 0.8 , respectively. FEA of jammed shelled specimens completes the picture of a cross section, illustrating that induced curvatures are symmetric about the midplane, regardless of c/b (Fig. 2h–j). As such, by purely geometric arguments, shelled specimens' cross sections decrease in their second moment of area so much when jammed that their k_j/k_{uj} would appear less than that of neat sheets (N^2). Experimentally we see that such is not the case. Subjecting the different shell designs to three-point bending and calculating initial stiffnesses via the slopes of the average force–displacement plots between 0 mm and 0.1 mm deflection (in the pre-slip regime for all samples), we discovered that all designs exceed k_j/k_{uj} of the neat control (Fig. 2k). Notably, c/b scales inversely to the stiffness differential, such that the shell with $c/b = 0.2$ peaks at a $5.4 \times$ greater stiffness ratio than that of the neat specimen (Fig. 2k).

To explain the shelled designs' amplified k_j/k_{uj} , we note the curvature-induced stiffness caused by in-plane strain in the thin sheets when jammed [32,33]. The energetic cost to stretch thin sheets scales as $\frac{h}{L}$, where L is the length of the sheet [34]. Since a jammed shelled specimen comprises inextensible sheets which already have pre-curvatures, transverse loads must overcome the prominent energetic hurdle of stretching the sheets to bend them about an axis misaligned with the pre-curvature. Induced curvatures thereby partially compensate for the stiffness lost through second moment of area decreases of the jammed cross section. Moreover, it would seem that second moment of area decreases impact stiffness more than the corresponding stiffness gains from curvature past a value of $c/b = 0.2$. Stiffness dependence on c/b can be likened to work on discretely clamped laminar jamming, in which it was found that decreasing clamp area reduces stiffness [35].

Besides c/b , another factor that governs initial flexural stiffness is jamming pressure. Subjecting a shelled specimen to three-point bending across a swath of vacuum values, we found that stiffness increases with the magnitude of vacuum (Fig. S5). This behavior stands in contrast to that of neat layers, which exhibit no stiffness change as a function of vacuum [19]. The coupling of initial stiffness to pressure in the shelled specimens can be attributed to the interplay of curvature-induced stiffness and contact interface area.

Based on jamming-induced curvature's impact on initial stiffness, we thought that it could also play a role in explaining some shelled specimens' persisting high forces at high deflections. For instance, whereas forces at high deflections for $c/b = 0.2$ resemble those of the neat control specimen, $c/b = 0.6$ and $c/b = 0.8$ cases are substantially elevated (Fig. 2l–n). Also observed in the $c/b = 0.6$ and $c/b = 0.8$ cases are sudden drops in force corresponding to curvature reversal of the shells (at low magnitudes of vacuum, negligible curvature is induced, and so no pronounced drop in force is evident; see Fig. S5). To understand how the induced curvature might impact a transition regime where slip occurs, we conducted FEA of jammed neat and shelled specimens in three-point bending (Note S2; Fig. S4). At the same value of deflection, 3% of the specimen's length, which is well into the fully-slipped regime for neat specimens, shelled simulations exhibit slip that occurs in smaller areas and is of less magnitude than that exhibited by a neat simulation. Increasing c/b sees slip occurring toward the outside walls of the shell and slipped regions decreasing in magnitude and area. Correspondingly, the contact pressure increases on the edges of the shell, suggesting that curvature diminishes the rate of slip by tightly holding the sheets together at the neutral axis.

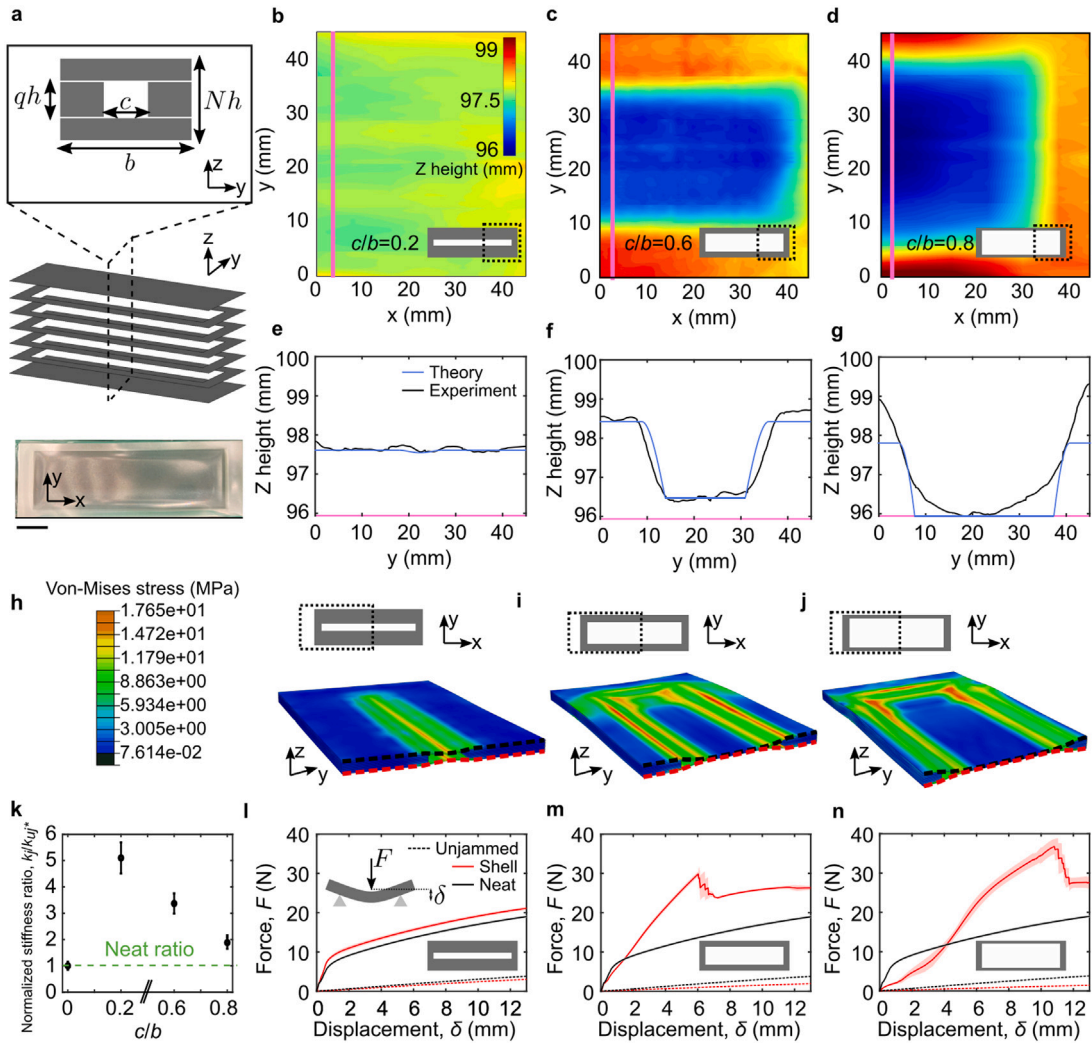


Fig. 2. Effect of shelling on laminar jamming. a. Schematic of shelled laminar jamming cross section labeling variables of interest. N is the number of layers, h is an individual layer's height, b is the width, c is the shell width, and q is the number of shelled layers. Below is an image of an actual jammed specimen with $c/b = 0.8$. Scale bar: 20.5 mm. b–d. Surface profilometry of a region of the specimens. Insets are to-scale illustrations of a shell layer, with dashed box indicating the section observed with surface profilometry. e–g. Cross section elevation plots corresponding to pink vertical lines in above profilometry images. Black lines are experimental data of the cross section shape; blue lines are theoretical predictions. h–j. FEA gives insight into the jammed specimens' cross section shapes. Shown are cross-sectional views of the jammed structures, with top (black) and bottom (red) unaltered layers highlighted. k. Jammed to unjammed initial stiffness ratio normalized by the neat specimen. The neat specimen results are plotted at $c/b = 0$. Error bars represent one standard deviation from the mean of five samples. l–n. Three-point bending results of jammed and unjammed specimens with $N = 15$ and $b = 50$. Different c of 10, 20, and 40 mm are made with optimal q (derived from the maximum of Eq. (4)) of 9, 11, and 11, respectively. Solid lines indicate a mean value of five trials; clouds indicate one standard deviation from the mean. (For interpretation of the references to color in this figure legend, the reader is referred to the web version of this article.)

Overall, by tuning the design variables c and q of the shelling operations, we found a method to increase k_j/k_{uj} , thwart the rate of slip, and thereby increase the high-deflection stiffness of laminar jamming systems. These desirable properties came in part from the induced curvature of the upper and lower shell boundaries upon jamming. Despite its advantages, the induced curvature poses issues for move-and-hold applications. Indeed, jamming shelled specimens after bending them length-wise into 180° arcs spontaneously forces them flat, owing to the induced curvature opposite the bending direction and the fact that the sheets cannot accommodate double curvatures (Video S1). We were thus prompted to explore methods to achieve improved move-and-hold performance while retaining the stiffness benefits of shelled layers.

1.3. Distributed voids and cuts

As a first attempt to mitigate spontaneous flattening of bent shelled specimens upon jamming while retaining high flexural stiffness ratios,

we sought to isolate induced curvatures to locally shelled regions, *i.e.* distributed voids. Specimens with distributed voids contain two distinct cross sections periodically spaced along their length: unaltered layers, or shelled layers (Fig. 3a). Distributed voids can be oriented with induced curvatures primarily along the same axis as bending deformation, or perpendicular to it, by tuning the ratio between the void depth, d , and a constant cut dimension, c . For example, $c/d = 1$ parameterizes a square void; $c/d > 1$ or $c/d < 1$ accordingly parameterize a rectangular void with its greater dimension along the width or length of the specimen, respectively. For designs abiding by either of these inequality cases, we hypothesized that distributed voids would (i) prevent curvature reversal propagation along the entire structure by serving as energetically stable regions; (ii) decrease the magnitude of induced curvature in void boundaries during jamming, and thereby prevent large reductions in the second moment of area.

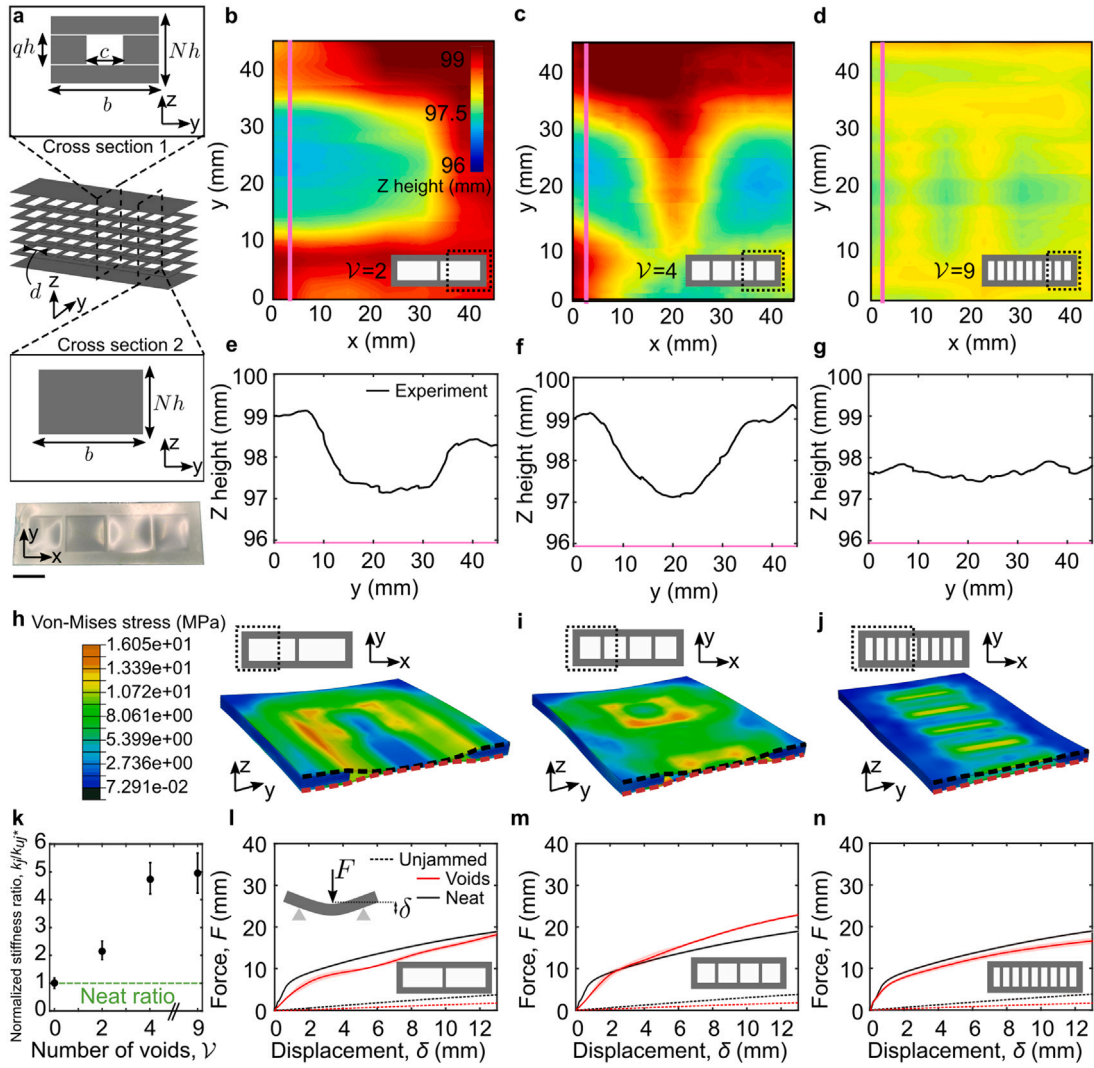


Fig. 3. Effect of distributed voids on laminar jamming. **a.** Schematic of the multiple cross sections associated with voided laminar jamming, labeling variables of interest. N is the number of layers, h is an individual layer's height, b is the width, c is the shell width, d is the shell depth along the length, and q is the number of shelled layers. Below is an image of an actual jammed specimen with $\nu = 0.4$. Scale bar: 20 mm. **b–d.** Surface profilometry of a region of specimens with different void numbers of $\nu = 2, 4,$ and 9 . Insets are to-scale illustrations of an augmented layer. **e–g.** Cross section elevation plots corresponding to pink vertical lines in above profilometry images. Black lines are experimental data of the cross section shape. **h–j.** FEA give insight into the jammed specimens' cross section shapes. Shown are cross-sectional views of the jammed structures, with top (black) and bottom (red) unaltered layers highlighted. **k.** Jammed to unjammed initial stiffness ratio normalized by the neat specimen (plotted at number of voids = 0). Error bars represent one standard deviation from the mean of five samples. **l–n.** Three-point bending results of jammed and unjammed specimens with $N = 15$ and $b = 50$. Solid lines indicate a mean value of five trials; clouds indicate one standard deviation from the mean. (For interpretation of the references to color in this figure legend, the reader is referred to the web version of this article.)

To ascertain the effect of d and the corresponding axis of induced curvature in furnishing stable surface regions, we conducted profilometry on specimens with a certain number of voids, ν , separated by unaltered sections of a fixed width. In particular, we studied $\nu = 2, 4,$ and 9 cases. q was held constant at 11 layers. For $\nu = 2$, induced curvature mainly arises perpendicular to the axis of bending, as with shelled specimens. For $\nu = 4$ and 9 , induced curvature mainly manifests along the axis of bending. Profilometry of the jammed specimens confirms that, through voids, we were able to both localize and reduce the amount of curvature along target axes relative to purely shelled specimens (Fig. 3b–d). For instance, the $\nu = 4$ specimen deflects a maximum of 1.7 mm in z when jammed, compared to 2.1 mm and 3 mm for the $c/b = 0.6$ and 0.8 shells, respectively. Plotting the deflection of the top layer in each specimen shows how curvature decreases with increasing ν (Fig. 3e–g). FEA likewise confirms that the cross-section shape morphs less with increasing ν (Fig. 3h–j). Thus, for high ν , we can reap the benefits of high stiffness differentials by mitigating decreases in the second moment of area due to curvature.

We conducted three-point bending on the specimens and calculated stiffness from the slopes of the average force–displacement plots between 0 mm and 0.1 mm deflection (in the pre-slip regime). The unjammed state of the specimens exhibited, on average, over 70% lower stiffness than that of the neat control, effectively elevating k_j/k_{uj} of all voided specimens relative to the neat control (Fig. 3k). Crucially, k_j/k_{uj} increases with ν , suggesting our strategy to mitigate second moment of area decreases by discretizing shells into voided sections was successful. The force–displacement responses of the samples when jammed demonstrate similar qualitative behavior to the neat control—defined pre-slip, transition, and fully-slipped regimes. More importantly, no rapid drop in force associated with curvature reversal is seen (Fig. 3l–n).

Topologically augmenting the specimens to create voids proved to be a viable method for enabling move-and-hold shape retention. Conducting the same format of experiment in which we bent jamming specimens into 180° arcs, we found that $\nu = 4$ and $\nu = 9$ retained the shape (Video S1). The $\nu = 2$ specimen did not, however, partially snapping back to a flat configuration upon jamming. We attribute this

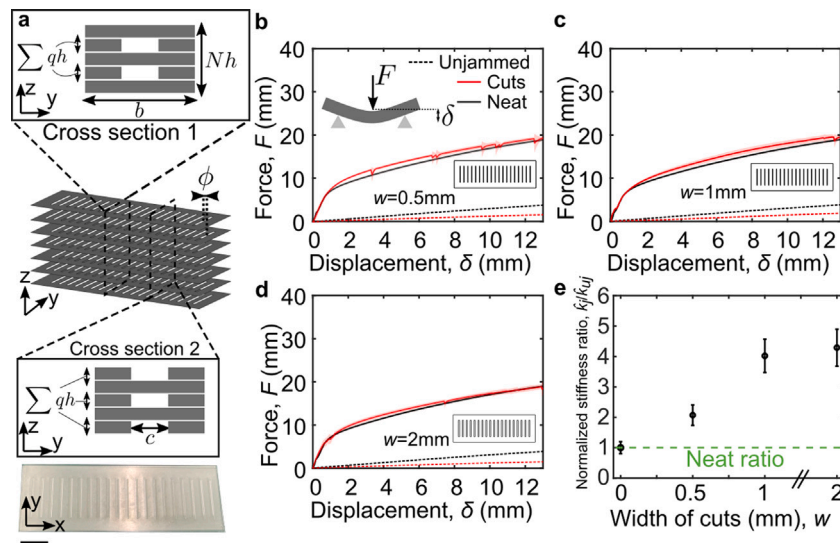


Fig. 4. Effect of offset cuts on laminar jamming. a. Schematic of the multiple cross sections associated with offset cutting operations, labeling variables of interest. N is the number of layers, h is an individual layer's height, b is the width, c is the cut width, ϕ is the offset spacing between centers of cuts in every other layer, and $\sum q$ is the number of cut layers in a given cross section along the length. Below is an image of an actual jammed specimen with $w = 1$ mm. Scale bar: 20 mm. b–d. Three-point bending results of jammed and unjammed specimens with $N = 15$ and $b = 50$. Different cut dimensions of $c = 0.5, 1,$ and 2 mm are shown. Insets are to-scale illustrations of an augmented layer. Solid lines indicate a mean value of five trials; clouds indicate one standard deviation from the mean. e. Jammed to unjammed initial stiffness ratio normalized by the neat specimen (plotted at $c = 0$). Error bars represent one standard deviation from the mean of five samples.

result to the fact that bending deformation must be sustained when jammed mostly at the hinges separating the voids. A single hinge is not sufficient to sustain the magnitude of bending deformation. The primary performance difference between the $\mathcal{V} = 4$ and $\mathcal{V} = 9$ samples was the continuity of held bending angles. Whereas $\mathcal{V} = 4$ expectantly created four discrete straight sections upon jamming, $\mathcal{V} = 9$ allowed for more continuous bending, manifesting not only at the hinges but also at the extremities of voided portions, due to their diminished d and thereby lower curvature-induced stiffness.

Another avenue we explored to achieve high k_j/k_{uj} and enhance the continuity of bending angles upon jamming relative to voided specimens was offset slender cuts. To create a laminar jamming system with offset cuts, we used two types of layers, each having 20 incisions of width w . The difference between the layers is a phase offset, ϕ between every other layer's cuts, giving rise to cross sections where gaps in the layers alternate (Fig. 4a; Note S3).

Three-point bending tests show force–displacement relations comparable to those of specimens with voids. Stiffnesses were calculated from the slopes of the average force–displacement plots between 0 mm and 1 mm deflection (in the pre-slip regime). Especially for smaller w , noise in the curves arises from sudden small drops and subsequent increases in force due to stick–slip interactions between edges of cuts (Fig. 4b–d). Due to no induced curvatures, the effect of curvature is decoupled from initial stiffness calculations. Correspondingly, k_j/k_{uj} increases with increasing w , as would be predicted by theory assuming an undeformed cross section (Fig. 4e). Move-and-hold performance was also enhanced. All samples made with offset cuts were able to move-and-hold to the prescribed bending angle of 180° (Video S1).

2. Applications

The three topological augmentation primitives characterized above – shells, voids, and cuts – provide a toolbox of techniques for programmed laminar jamming behavior with applications ranging from deployable structures to robotics. As a simple testament to the new shape-matching abilities afforded by linear cuts, we first created perforated jamming systems that fold to match discontinuous three-dimensional (3D) shapes, like a tetrahedron and a cube (Fig. 5a; Video S2). Perforations act as hinges at specified regions of the developed surface, allowing folding to sharp edges. This property stands

in contrast to neat sheets, whose thickness precludes folding to sharp edges and instead, enforces smooth curvatures. Under compression, the faceted tetrahedron and cube exhibit higher global stiffnesses and are able to support $2\times$ and $5\times$ greater loads than their smooth counterparts, respectively. Perforations allow faceted shapes to retain the relative configurations of their faces, reinforcing structural stiffness.

Second, we harnessed kirigami alterations to enhance move-and-hold operations for load-bearing. Tuning the second moment of area while avoiding the instabilities of induced curvature, we achieved a radical increase in k_j/k_{uj} for cut and voided sheets relative to neat sheets. Kirigami layer jamming specimens held an imposed bending of 180° and supported weight $36\times$ greater than their own with negligible deflection (Fig. 5b; Video S1). The analogous neat specimen, on the other hand, could not hold the bending deformation and collapsed under the same applied weight.

Third, we leveraged a meander cut pattern to fabricate contiguous jamming sheets with bi-axial strain relief. A stack of these sheets was used to realize stretchable laminar jamming, and successfully conformed to doubly-curved surfaces of a 3D-printed face and a toy car (Fig. 5c, Video S3). The shape matching of the kirigami sheets was substantially better than that of neat sheets, though the meander pattern had limits in terms of the resolution of features it could accommodate. Details on the face are clearly evidenced in the kirigami laminar jamming system, but more nuanced features of the toy car, such as the ridges and gaps between the wheels and chassis, are lost. Further shrinking the meander would offer a way to capture such fine details. Kirigami techniques thus provide a scalable and rapid alternative to stretchable layer jamming, which normally requires tedious fabrication of discrete, interleaved sub-units [27].

Lastly, we created shape-morphing jamming structures by stacking multiple voided specimens with varying induced curvature directions. As one example, elastic frustration caused by the interface of stacked opposite-curvature shells forces the assembly to assume a doubly-curved midplane [36] (Fig. 5d; Video S4). The arising saddle shape demonstrates how sheets of zero Gaussian curvature, when altered via kirigami, can collectively equilibrate to Gaussian curved topography. Compared to existing shape-morphing structures using vacuum [37, 38], kirigami layer jamming allows for realization of doubly-curved surfaces in addition to a high degree of stiffness tunability, boding well for future robotics applications from manipulation to mechanical camouflage.

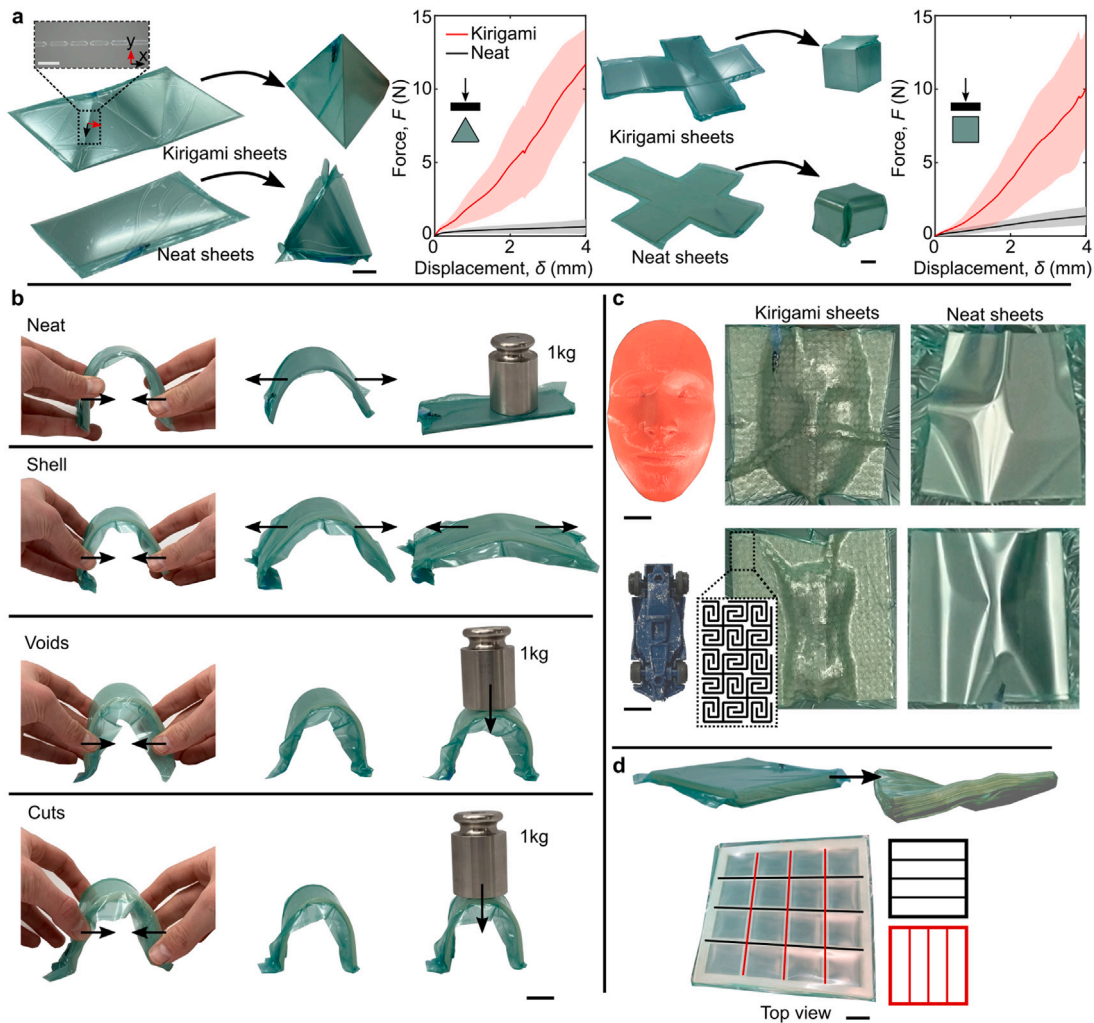


Fig. 5. Demonstrations of kirigami layer jamming. **a.** In contrast to neat layers, perforations allow move-and-hold operations to match 3D shapes with discontinuities, such as a tetrahedron and cube. Both neat and kirigami examples have the same number of layers $N = 10$ and sheet thicknesses $h = 0.1$ mm. Scale bars: 20 mm. Plots show force–displacement responses of the 3D shapes under compressional loading. Solid lines represent an average of five trials; error clouds represent one standard deviation from the mean. Optical micrograph inset scale bar: 2 mm. **b.** Bending specimens to 180° and jamming to assess move-and-hold performance. Load bearing over $36 \times$ a specimen's own weight can be achieved by kirigami sheets that use distributed cuts or voids. On the other hand, the restoring bending force of the neat specimen makes it unable to support the load, and the shelled specimen undergoes spontaneous curvature reversal, forcing it flat. Scale bar: 25 mm. **c.** Kirigami cuts provide bi-axial strain relief, allowing facile creation of stretchable laminar jamming systems. Here, we approximate the doubly-curved surfaces of a face and toy car. Neat sheets are unable to capture the complexity of the surfaces. Scale bars: 13 mm (top); 19 mm (bottom). **d.** Curvature induced by voids can be harnessed to create elastically frustrated shape-morphing jamming structures. In this example, we use $N = 30$. Two unaltered layers on top and bottom sandwich 14 shelled layers tailored to induce curvature in either of two principal directions (red and black schematics of the shell layers is indicated in figure). Scale bar: 15 mm. (For interpretation of the references to color in this figure legend, the reader is referred to the web version of this article.)

3. Concluding remarks

We presented kirigami layer jamming, a straightforward way to topologically augment sheets in laminar jamming systems to elicit desired mechanical properties. We focused on three augmentation primitives: shells, voids, and cuts. Each boasted their own performance-enhancing qualities. Shelling radically increased specimens' jammed-to-unjammed flexural stiffness ratios, and combatted slip at high deflections due to induced curvatures under jamming. However, this same useful quality diminished the utility of shelling in move-and-hold applications, because imposed bending deflections reversed the curvature upon jamming, forcing the system back flat. Since move-and-hold performance is governed by the competition between a deformed specimens' restoring spring force and the cohesion force due to jamming, we explored other kirigami primitives to augment these quantities at different rates. Voids presented a compromise between high jammed to unjammed stiffness ratio and move-and-hold capability by mitigating curvature reversal through energetically stable regions of surface.

Further exploration led us to study offset cuts that completely removed undesired effects of induced curvature, enabling continuous move-and-hold performance and retention of desirable stiffness ratios (See Note S4 for a tabulation of all designs' stiffness values and jammed-to-unjammed ratios).

Different demonstrations employing laminar jamming systems with the above kirigami primitives showcase new capabilities: discontinuous shape-matching, enhanced load-bearing, pressure-induced shape-morphing, and doubly-curved surface matching with contiguous sheets. Looking forward, we envision kirigami layer jamming will prove especially useful in all manner of move-and-hold robotic applications where energy consumption is a concern, such as untethered variable stiffness continuum manipulators, robotic appendages, and assistive exosuits. Topological augmentations can reduce the unjammed stiffness of sheets, diminishing the required force of an actuator to move it to a desired configuration, yet simultaneously preserving jammed stiffness requisite to load-bearing applications.

Beyond the scope of this manuscript, there are still many kirigami patterns to evaluate and other aspects of jamming performance to

optimize through geometry. For instance, we did not consider tensile or torsional stiffnesses in the present work. Tuning the frictional qualities of the sheets through cutting, or creating jamming-induced interlocking mechanisms with shells might increase tensile stiffness. Lastly, we foresee the geometric concepts employed herein to amplify laminar jamming systems' properties translating to other jamming systems with different constituent form factors. It may be possible, for example, to amplify the bending response of fiber jamming by inducing hierarchical curvatures within the fiber bundle. Overall, kirigami layer jamming unveils an immense design space for variable stiffness materials that we set the foundation for in this manuscript.

Declaration of competing interest

The authors declare that they have no known competing financial interests or personal relationships that could have appeared to influence the work reported in this paper.

Data availability

Data will be made available on request.

Acknowledgments

We thank Medha Goyal for assistance with mathematical derivations. This project was sponsored by the Office of Naval Research, United States under award N00014-21-1-2417. Any opinions, findings, and conclusions or recommendations expressed in this material are those of the authors and do not necessarily reflect the views of the Office of Naval Research.

Appendix A. Supplementary data

Supplementary material related to this article can be found online at <https://doi.org/10.1016/j.eml.2023.102084>.

References

- [1] D. Zappetti, S.H. Jeong, J. Shintake, D. Floreano, Phase changing materials-based variable-stiffness tensegrity structures, *Soft Robot.* (2019) soro.2019.0091.
- [2] I.D. Falco, M. Cianchetti, A. Mencias, A soft multi-module manipulator with variable stiffness for minimally invasive surgery, *Bioinspiration Biomim.* 12 (5) (2017) 056008.
- [3] R. Baines, S.K. Patiballa, J. Booth, L. Ramirez, T. Sipple, A. Garcia, F. Fish, R. Kramer-Bottiglio, Multi-environment robotic transitions through adaptive morphogenesis, *Nature* 610 (7931) (2022) 283–289.
- [4] T.L. Buckner, R. Kramer-Bottiglio, Functional fibers for robotic fabrics, *Multifunct. Mater.* 1 (1) (2018) 012001.
- [5] L. Blanc, A. Delchambre, P. Lambert, Flexible medical devices: Review of controllable stiffness solutions, *Actuators* 6 (3) (2017) 23.
- [6] H. Rodrigue, W. Wang, B. Bhandari, M.-W. Han, S.-H. Ahn, SMA-based smart soft composite structure capable of multiple modes of actuation, *Composites B* 82 (2015) 152–158.
- [7] X. Huang, M. Ford, Z.J. Patterson, M. Zarepoor, C. Pan, C. Majidi, Shape memory materials for electrically-powered soft machines, *J. Mater. Chem. B* 8 (21) (2020) 4539–4551.
- [8] T.L. Buckner, M.C. Yuen, S.Y. Kim, R. Kramer-Bottiglio, Enhanced variable stiffness and variable stretchability enabled by phase-changing particulate additives, *Adv. Funct. Mater.* (2019) 1903368.
- [9] B.E. Schubert, D. Floreano, Variable stiffness material based on rigid low-melting-point-alloy microstructures embedded in soft poly(dimethylsiloxane) (PDMS), *RSC Adv.* 3 (46) (2013) 24671–24679.
- [10] R. Hinchet, H. Shea, High force density textile electrostatic clutch, *Adv. Mater. Technol.* 5 (4) (2020) 1900895.
- [11] S. Diller, C. Majidi, S.H. Collins, A lightweight, low-power electroadhesive clutch and spring for exoskeleton actuation, in: 2016 IEEE International Conference on Robotics and Automation, ICRA, IEEE, 2016, pp. 682–689.
- [12] B. Aktaş, Y.S. Narang, N. Vasios, K. Bertoldi, R.D. Howe, A modeling framework for jamming structures, *Adv. Funct. Mater.* 31 (16) (2021) 2007554.
- [13] V. Wall, R. Deimel, O. Brock, Selective stiffening of soft actuators based on jamming, in: 2015 IEEE International Conference on Robotics and Automation, ICRA, IEEE, Seattle, WA, USA, 2015, pp. 252–257.
- [14] A.A. Stanley, K. Hata, A.M. Okamura, Closed-loop shape control of a haptic jamming deformable surface, in: 2016 IEEE International Conference on Robotics and Automation, ICRA, 2016, pp. 2718–2724.
- [15] S. Chopra, M.T. Tolley, N. Gravish, Granular jamming feet enable improved foot-ground interactions for robot mobility on deformable ground, *IEEE Robot. Autom. Lett.* 5 (3) (2020) 3975–3981.
- [16] N.G. Cheng, M.B. Lobovsky, S.J. Keating, A.M. Setapen, K.I. Gero, A.E. Hosoi, K.D. Iagnemma, Design and analysis of a robust, low-cost, highly articulated manipulator enabled by jamming of granular media, in: 2012 IEEE International Conference on Robotics and Automation, 2012, pp. 4328–4333.
- [17] S.G. Fitzgerald, G.W. Delaney, D. Howard, A review of jamming actuation in soft robotics, *Actuators* 9 (4) (2020) 104.
- [18] N. Vasios, Y. Narang, B. Aktaş, R. Howe, K. Bertoldi, Numerical analysis of periodic laminar and fibrous media undergoing a jamming transition, *Eur. J. Mech. A Solids* 75 (2019) 322–329.
- [19] Y.S. Narang, J.J. Vlassak, R.D. Howe, Mechanically versatile soft machines through laminar jamming, *Adv. Funct. Mater.* 28 (17) (2018) 1707136.
- [20] J.L.C. Santiago, I.S. Godage, P. Gonthina, I.D. Walker, Soft robots and Kangaroo tails: Modulating compliance in continuum structures through mechanical layer jamming, *Soft Robot.* 3 (2) (2016) 54–63.
- [21] F. Caruso, G. Mantriota, L. Afferrante, G. Reina, A theoretical model for multi-layer jamming systems, *Mech. Mach. Theory* 172 (2022) 104788.
- [22] Y.S. Narang, B. Aktaş, S. Ornellas, J.J. Vlassak, R.D. Howe, Lightweight highly tunable jamming-based composites, *Soft Robot.* 7 (6) (2020) 724–735.
- [23] D.C.F. Li, Z. Wang, B. Ouyang, Y.-H. Liu, A reconfigurable variable stiffness manipulator by a sliding layer mechanism, in: 2019 International Conference on Robotics and Automation, ICRA, IEEE, Montreal, QC, Canada, 2019, pp. 3976–3982.
- [24] D.C.F. Li, Z. Wang, J. Zhou, Y.-H. Liu, Honeycomb jamming: An enabling technology of variable stiffness reconfiguration, *Soft Robot.* 8 (6) (2021) 720–734.
- [25] J. Kwon, I. Choi, M. Park, J. Moon, B. Jeong, P. Pathak, J. Ahn, Y.-L. Park, Selectively stiffening garments enabled by cellular composites, *Adv. Mater. Technol.* 7 (9) (2022) 2101543.
- [26] J. Ou, L. Yao, D. Tauber, J. Steimle, R. Niiyama, H. Ishii, jamSheets: thin interfaces with tunable stiffness enabled by layer jamming, in: Proceedings of the 8th International Conference on Tangible, Embedded and Embodied Interaction - TEI '14, ACM Press, Munich, Germany, 2013, pp. 65–72.
- [27] D.S. Shah, E.J. Yang, M.C. Yuen, E.C. Huang, R. Kramer-Bottiglio, Jamming skins that control system rigidity from the surface, *Adv. Funct. Mater.* (2020) 2006915.
- [28] L. Jin, A.E. Forte, B. Deng, A. Rafsanjani, K. Bertoldi, Kirigami-Inspired inflatables with programmable shapes, *Adv. Mater.* 32 (33) (2020) 2001863.
- [29] Y. Hong, Y. Chi, S. Wu, Y. Li, Y. Zhu, J. Yin, Boundary curvature guided programmable shape-morphing Kirigami sheets, *Nature Commun.* 13 (1) (2022) 530.
- [30] H. Cho, D.-N. Kim, Controlling the stiffness of bistable Kirigami surfaces via spatially varying hinges, *Mater. Des.* 231 (2023) 112053.
- [31] S. Kawamura, T. Yamamoto, D. Ishida, T. Ogata, Y. Nakayama, O. Tabata, S. Sugiyama, Development of passive elements with variable mechanical impedance for wearable robots, in: Proceedings 2002 IEEE International Conference on Robotics and Automation (Cat. No.02CH37292), Vol. 1, 2002, pp. 248–253 vol.1.
- [32] V. Pini, J.J. Ruz, P.M. Kosaka, O. Malvar, M. Calleja, J. Tamayo, How two-dimensional bending can extraordinarily stiffen thin sheets, *Sci. Rep.* 6 (1) (2016) 29627.
- [33] M. Venkadesan, A. Yawar, C.M. Eng, M.A. Dias, D.K. Singh, S.M. Tommasini, A.H. Haims, M.M. Bandi, S. Mandre, Stiffness of the human foot and evolution of the transverse arch, *Nature* 579 (7797) (2020) 97–100.
- [34] T.A. Witten, Stress focusing in elastic sheets, *Rev. Modern Phys.* 79 (2007) 643–675.
- [35] Y. Zhou, L.M. Headings, M.J. Dapino, Discrete layer jamming for variable stiffness co-Robot arms, *J. Mech. Robot.* 12 (1) (2020) 015001.
- [36] I. Levin, E. Siefert, E. Sharon, C. Maor, Hierarchy of geometrical frustration in elastic ribbons: Shape-transitions and energy scaling obtained from a general asymptotic theory, *J. Mech. Phys. Solids* 156 (2021) 104579.
- [37] M.A. Robertson, J. Paik, New soft robots really suck: Vacuum-powered systems empower diverse capabilities, *Science Robotics* 2 (9) (2017) eaan6357.
- [38] X. Liu, Z. Liang, Soft actuator using sponge units with constrained film and layer jamming, in: *Industrial Robot: The International Journal of Robotics Research and Application*, Vol. 49, No. 4, Industrial Robot (2022) 616–624.